https://doi.org/10.5194/acp-2020-902
Preprint. Discussion started: 2 November 2020

Dynamic Processes Dominating Ozone Variability in Warm Seasons of 2014–2018 over the Yangtze River Delta Region, China

Da Gao[1], Min Xie[1*], Jane Liu[2,3], Tijian Wang[1], Chaoqun Ma[1,a], Haokun Bai[1], Xing Chen[1]

[1] School of Atmospheric Sciences, Joint Center for Atmospheric Radar Research of CMA/NJU, CMA-NJU Joint Laboratory for Climate Prediction Studies, Jiangsu Collaborative Innovation Center for Climate Change, Nanjing University, Nanjing 210023, China

[2] College of Geographic Sciences, Fujian Normal University, Fuzhou 350007, China

[3] Department of Geography and Planning, University of Toronto M5S 3G3, Canada

[a] now at: Minerva Research Group, Max Planck Institute for Chemistry, Mainz, Germany

----

* Corresponding author. School of Atmospheric Sciences, Nanjing University, Nanjing 210023, China. minxie@nju.edu.cn (M. Xie)

Abstract: Ozone (O_3) pollution is of great concern in the Yangtze River Delta (YRD) region of China, and the regional O_3 pollution is closely associated with dominant weather systems. With a focus on the warm seasons (April–September) from 2014 to 2018, we quantitatively analyze the characteristics of O_3 variations over the YRD, the impacts of large-scale and synoptic-scale circulations on the variations and the associated meteorological controlling factors, based on observed ground-level O_3 and meteorological data. Our analysis suggests an increasing trend of the regional mean O_3 concentration in the YRD at 1.81 ppb per year over 2014-2018. Spatially, the empirical orthogonal function (EOF) analysis suggests the dominant mode accounting for 65.70% variation in O_3, implying that an increase in O_3 is the dominant tendency in the entire YRD. Meteorology is estimated to increase the regional mean O_3 concentration by 2.81 ppb at most from 2014 to 2018. Relative humidity is found to be the most influential meteorological factor impacting O_3 concentration. As the atmospheric circulation can affect local meteorological factors and O_3 levels, we identify five dominant synoptic weather patterns (SWPs) in the warm seasons in the YRD using the t-mode principal component analysis (PTT) classification. The typical weather systems of SWPs include western Pacific Subtropical High (WPSH) under SWP1, a continental

https://doi.org/10.5194/acp-2020-902
Preprint. Discussion started: 2 November 2020

Atmospheric Chemistry and Physics Discussions

high under SWP2, an extratropical cyclone under SWP3, a southern low pressure and WPSH under SWP4 and the north China anticyclone under SWP5. The annual variations of all five SWPs are favorable to the increase in O_3 concentrations over 2014-2018. Moreover, the change in SWP intensity contributes more to the O_3 inter-annual variation than the SWP frequency change. The SWP intensity change includes the weakening and northward-extending of the western Pacific subtropical high (WPSH) under SWP1, the weakening of the continental high under SWP2, an extratropical cyclone strengthening under SWP3, the southern low pressure weakening and WPSH weakening under SWP4, and the north China anticyclone weakening under SWP5. All these changes prevent the water vapor in the southern sea from being transported to the YRD, and increase air temperature in the YRD. In addition, the descending motions strengthen in the YRD located behind the trough and in front of the ridge due to the strengthening of the ridge and trough in the westerlies. Then, the strengthened descending motion leads to less cloud cover and strong solar radiation, which are favorable to O_3 formation and accumulation. Finally, we reconstruct an EOF mode 1 time series that shows high correlation with the original O_3 time series, and the reconstructed time series performs well in defining the change in SWP intensity according to the unique feature under each of the SWPs.

1. Introduction

As an air pollutant, surface ozone (O_3) is harmful to human health and vegetation growth, such as damaging human lungs (Jerrett et al. 2009; Day et al. 2017) and destroying forest and agricultural crops (Yue et al. 2017). In recent years, after reducing the emissions following "Thirteenth Five-Year Plan" Comprehensive Work Plan for Energy Saving and Emission Reduction since 2016, concentrations of many pollutants have decreased over the past few years in China, but not for O_3. Furthermore, heavy O_3 pollutions occur more frequently and more severely in China than those in Japan, South Korea, Europe and the United States (Lu et al. 2018). Li et al. (2018) proposed that the rapid decrease of fine particulate matter (PM) in China is a reason for such O_3 increase by slowing down the aerosol sink of hydro-preoxy radicals. Yet, the contribution of meteorological factors to the O_3 increase is unclear.

Surface O_3 is mainly formed through complex and nonlinear photochemical reactions of volatile organic compounds (VOCs) and nitrogen oxides (NO_x) exposed to the sunlight. Ozone

https://doi.org/10.5194/acp-2020-902
Preprint. Discussion started: 2 November 2020

formation is sensitive to concentrations of NO_x and VOCs, i.e., O_3 formation can be NO_x-limited or VOC-limited regimes depending on concentrations of NO_x and VOCs (Xie et al. 2014; Jin and Holloway 2015). Meteorology could also affect O_3 levels through modulation of photochemical reactions, advection, convection and turbulent transport, as well as dry and wet depositions (Liu et al. 2013). Synoptic weather patterns (SWPs) and the associated meteorological conditions can impact long-term and daily O_3 variations. Understanding the mechanisms of meteorological influences on O_3 variations and quantifying such influences would help provide effective emission-controlling plans for O_3 pollution.

Severe O_3 pollution episodes are accompanied with specific local meteorological conditions, such as high temperature, strong solar radiation, drying condition and stagnant weather (Jacob and Winner 2009; Doherty et al. 2013; Pu et al. 2017; Zhang et al. 2018). Moreover, local meteorological conditions are often related to specific synoptic-scale and large-scale atmospheric circulation systems. For example, O_3 pollution in the eastern United States is notably influenced by the cyclone frequency (Leibensperger et al. 2008), latitude of the polar jet over eastern North America (Barnes and Fiore. 2013) and the behavior of the quasi-permanent Bermuda High (Fiore et al. 2003, Wang et al. 2016). In China, Yang et al. (2014) illustrated that the changes in meteorological parameters, associated with the East Asian summer monsoon, lead to 2–5 % inter-annual variations in surface O_3 concentrations over the central-eastern China. Zhao and Wang et al. (2017) found that a significantly strong western Pacific subtropical high (WPSH) could result in higher relative humidity (RH), more clouds, more rainfall, and less ultraviolet radiation, finally leading to less O_3 formation. Using model simulation, Shu et al. (2016) investigated the synergistical impact of the WPSH and typhoon on O_3 level in Yangtze River Delta region.

As known, a region is influenced by different weather systems. Weather classification, as a way to distinguish the different large-scale and synoptic-scale atmospheric circulation systems, is widely used in exploring connections between weather patterns and O_3 levels (Han et al. 2020; Gao et al. 2020). Gao et al. (2020) discussed influences of SWPs on O_3 levels, and revealed differences in O_3 pollution levels due to the minor changes in atmospheric circulations. However, spatially, it is uncertain that how the change in SWPs could lead to O_3 pollution in detail,

https://doi.org/10.5194/acp-2020-902
Preprint. Discussion started: 2 November 2020

especially in the YRD. For the northern China and the PRD region, Liu et al. (2019) quantified the impact of synoptic circulation patterns on O_3 variability in the northern China from April to October during 2013–2017. Yang et al. (2019) quantitatively assessed the impacts of meteorological factors and the precursor emissions on the long-term trend of ambient O_3 over the PRD region. Yet, whether variations in SWPs can lead to O_3 increases has not be sufficiently addressed.

Due to the ever-growing O_3 level in the YRD (Tong et al. 2017; Gao et al. 2017), the studies on characteristics of O_3 variation and the underlying mechanisms for the variation are urgently required. To this end, here the O_3 variations in space and time, as well as 5-year trend, in the YRD is quantitatively investigated, and the mechanisms of meteorological influences on the O_3 variations are analyzed. Especially, the characteristics of the corresponding SWPs are discussed in detailed. The remainder of this paper is organized as follows. Data and methods are introduced in section 2. The inter-annual variation and 5-year trend and spatial variation characteristics are illustrated in section 3.1. The impact of meteorological factors on the O_3 variation is discussed in section 3.2. The main SWPs and the effects of their change on the O_3 variation are described in section 3.3. Section 3.4 discusses the contributions of the SWP intensity and frequency change to the inter-annual variation and trend of O_3. Finally, the conclusion and discussions are shown in section 4.

2. Data and methods

2.1. O_3 and meteorological datasets

The maximum daily 8-hours average O_3 data are available from the National Environmental Monitoring Center of China, which were acquired from the air quality real-time publishing platform (http://106.37.208.233:20035). The hourly observation data of meteorological factors including air temperature (T), RH, wind speed (WS) and sunshine duration (SD) in the warm seasons from April to September over 2014–2018 were acquired from the National Meteorological Center of China Meteorological Administration (http://eng.nmc.cn). 26 cities are selected as typical cities representative of the YRD according to the “Urban agglomeration on Yangtze River Delta” approved by China’s State Council in 2016. In this paper, the term "O_3 concentration" refers to the maximum daily 8-hours average O_3 concentration unless stated otherwise.

2.2. Linear trend analyses

In order to characterize the O_3 variation in the warm seasons during 2014–2018 over the YRD, a linear trend method based on monthly anomalies is used (see Equation 1), which has been widely used to calculate the trends of time series with seasonal cycles and autocorrelation. The O_3 monthly anomalies are more precise than O_3 monthly means because of the reducing impact of missing data. Using this method, Cooper et al. (2020) and Lu et al. (2020) quantified the O_3 trend in 27 globally distributed remote locations and the whole China. In addition, anomalies of monthly average O_3 concentration are defined as the difference between the individual monthly mean and the monthly mean of 2014–2018. The parametric linear trend is calculated by using the generalized least-squares method with auto-regression.

$$y_t = b + kt + \alpha \cos\left(\frac{2\pi M}{6}\right) + \beta \sin\left(\frac{2\pi M}{6}\right) + R_t \qquad (1),$$

where y_t represents the monthly anomaly, t is the monthly index from April to September during 2014–2018, b denotes the intercept, k is the linear trend, α and β are coefficients for a 6-month harmonic series (M ranges from 1 to 6) which is used to account for potentially remaining seasonal signals, and R_t represents a normal random error series.

2.3. Meteorological adjustment

The meteorological adjustment, a statistical method, is applied to quantify the impact of meteorology on O_3 variation through removing such impact in the original O_3 data. It is similar to a model simulation that keeps the emission levels fixed but allows meteorology to vary. Yet, this method requires much less computing resources than a model simulation. The method is introduced in detail as follows.

In the meteorological adjustment, the observed O_3 and meteorological data are separated into long-term, seasonal, and short-term data (Rao and Zurbenko 1994a, b). The Kolmogorov-Zurbenko (KZ) filter can be expressed as follows.

$$R(t) = L(t) + S(t) + W(t) \qquad (2),$$

where $R(t)$ represents the raw time series data, $L(t)$ the long-term trend on a timescale of years, $S(t)$ the seasonal variation on a timescale of months, and $W(t)$ the short-term component on a

https://doi.org/10.5194/acp-2020-902
Preprint. Discussion started: 2 November 2020

timescale of days.

In order to remove the high-pass signal, the KZ filter carries out *p* times of iterations of a moving average with the window length *m*, which is defined as

$$Y_i = \frac{1}{m}\sum_{j=-k}^{k} R_{i+j} \qquad (3)$$

where *R* is the original time series, *i* an index for the time of iteration, *j* an index for sampling inside the window, and *k* the number of sampling on one side of the window. The window length $m = 2k + 1$. *Y* is the input time series after one iteration. Different scales of motions are obtained by changing the window length and the number of iterations (Milanchus et al. 1998; Eskridge et al. 1997). The filter periods of less than N days can be calculated with window length m and the number of iteration p, as follows:

$$\mathrm{m} \times p^{\frac{1}{2}} \le N \qquad (4).$$

Therefore, the cycles of 33 days can be removed by a KZ (15, 5) filter with the window length of 15 and 5 iterations. In the following equation 5, BL(t) is the O_3 and meteorological time series obtained by KZ(15,5) filter and refers to their baseline variations which are the sum of the long term L(t) and the seasonal component S(t)..

$$BL(t) = KZ_{(15,5)} = L(t) + S(t) = KZ_{(183,3)} + S(t) \qquad (5).$$

The long-term trend is separated from the raw data obtained by KZ (183, 3) with the periods of > 632 days, and then the seasonal and the short-term component $W(t)$ can be defined as

$$S(t) = KZ_{(15,5)} - KZ_{(183,3)} \qquad (6),$$

$$W(t) = \mathrm{X(t)} - \mathrm{BL(t)} = \mathrm{X(t)} - KZ_{(15,5)} \qquad (7).$$

After KZ filtering, the meteorological adjustment is conducted by the multivariate regression between the O_3 concentration and meteorological factors such as T, RH, wind speed and sunshine duration (Wise and Comrie 2005; Papanastasiou et al. 2012).

$$A_{BL}(t) = a_{BL} + \sum b_{BLi} \cdot M_{BLi} + \epsilon_{BL}(t) \qquad (8),$$

$$A_W(t) = a_W + \sum b_{Wi} \cdot M_{Wi} + \epsilon_W(t) \qquad (9),$$

$$\epsilon(\mathrm{t}) = \epsilon_{BL}(t) + \epsilon_W(t) \qquad (10),$$

$$A_{ad}(t) = \epsilon(t) + \sum b_{BLi} \cdot \overline{M}_{BLi} + \sum b_{Wi} \cdot \overline{M}_{Wi} + a_{BL} + a_W \qquad (11).$$

the multivariate regression models between baseline and short-term O_3 and meteorological factors are shown in equations 8 and 9. The $A_{BL}(t)$ and M_{BLi} represent the sum of the long term L(t) and the seasonal component S(t) of O_3 concentration and meteorological factors. The $A_W(t)$ and M_{Wi} represent the short-term W(t) of O_3 concentration and meteorological factors. The a and b are the fitted parameters, and i is time point (days). $\epsilon(t)$ is the residual term. The average meteorological condition $\overline{M}$ at the same calendar date during the 5 years is regarded as the base condition for that date, and the meteorological adjustment is conducted against the base condition. By these steps, $A_{ad}(t)$ refers to the meteorologically adjusted O_3 variation with the homogenized annual variation in meteorological conditions. The difference between raw O_3 time series and $A_{ad}(t)$ represents the meteorological impact.

2.4. Classification of SWPs

In order to find the detailed variation characteristics of SWPs, we first extract the predominant SWPs in the warm seasons over the YRD using a weather classification method. Common objective classification methods include using predefined type, the leader algorithm, the cluster analysis, optimization algorithms and eigenvectors (Philipp et al. 2016). The PTT method, a simplified variant of t-mode principal component analysis using orthogonal rotation, is used to classify SWPs during 2014–2018. It is one of the methods for weather classification in European Cooperation in Science and Technology Action 733 (Philipp et al. 2016), which is widely used in atmospheric sciences (Hou et al. 2019).

2.5. FNL and ERA-Interim meteorological data

The National Center for Environmental Prediction Final Operational Global Analysis (FNL) data (http://rda.ucar.edu/datasets/ds083.2/) produced by the Global Data Assimilation System are used in classifying SWPs and analyzing atmospheric circulations. The data have a horizontal resolution of 2.5°×2.5°, with 144×73 horizontal grids available every 6 hours. From the near surface layer to 10 hPa, there are 17 pressure levels in the vertical direction. The data of the geopotential height and wind at 500 hPa and 850 hPa, the vertical wind (Ω), T and RH are used in this study. At the same time, the total cloud cover (TCC) and solar radiation (SR) from ERA-interim are supplemented in this study, which have the same temporal and spatial resolutions as the FNL data.

The FNL geopotential height field at 850 hPa can capture the synoptic circulation variations over the YRD well (Shu et al. 2017). In this study, we use the geopotential height at 850 hPa from April to September during 2014–2018 as the input for the PTT.

2.6. Reconstruction of O_3 concentration based on SWP

To quantify the inter-annual variability captured by the variations (frequency and intensity) in the synoptic weather patterns, Yaranl (1992) provided an algorithm to find the contribution of SWP frequency variation to the inter-annual O_3 variation. The specific calculation is as follows.

$$\overline{\overline{O_{3m}}}(fre) = \sum_{k=1}^{6} \overline{O_{3k}} F_{km} \qquad (12),$$

where $\overline{\overline{O_{3m}}}(fre)$ is the reconstructed mean O_3 concentration influenced by the frequency variation in SWPs from April to September for year m, $\overline{O_{3k}}$ is the 5-year mean O_3 concentration for SWP k, and F_{km} is the occurrence frequency of SWP k during April–September for year m.

Hegarty et al. (2007) suggested that changes in the SWP include both frequency change and intensity change. The intensity of SWPs represents the location and strength of the weather system. Moreover, they noted that the environmental and climate-related contributions to the inter-annual variations of O_3 could be better separated by considering these two changes. So, Equation12 is modified into the following form.

$$\overline{\overline{O_{3m}}}(fre + int) = \sum_{k=1}^{6} (\overline{O_{3k}} + \Delta O_{3km}) F_{km} \qquad (13),$$

where $\overline{\overline{O_{3m}}}(fre + int)$ is the reconstructed average O_3 concentration influenced by the frequency and intensity changes of SWPs from April to September for year m; ΔO_{3km} is the modified difference on the fitting line, which is obtained through a linear fitting of the annual O_3 concentration anomalies (ΔO_3) to the SWP intensity index (SWPII) for SWP k in year m. ΔO_{3km} represents the part of the annual observed O_3 oscillation caused by the intensity variation in each SWP. Hegarty et al. (2007) used the domain averaged sea level pressure to represent the circulation intensity index (CII). Liu et al. (2019) reconstructed the inter-annual O_3 level in the northern China using the center pressure of the lowest pressure system. But we find the intensity variation in each SWP is different when O_3 increases. So we select different SWPII under each pattern according to the characteristics of high O_3 concentration. Lastly, we select the maximum height in zone-1 (25 °N–40 °N, 110 °E–130 °E), the maximum height in zone-2 (20 °N–50 °N,

https://doi.org/10.5194/acp-2020-902
Preprint. Discussion started: 2 November 2020

90 °E–140 °E) and the mean height in zone-3 (10 °N–40 °N, 110 °E–130 °E). Detailed demonstration is introduced in section 3.5.

3. Results and discussion

3.1. Spatio-temporal variations of O_3 in the YRD region

3.1.1. Inter-annual variations of O_3

Fig. 1a shows the time series of the anomalies of the monthly mean O_3 concentration over the YRD from April to September during 2014–2018, as well as the corresponding linear fitting curve. Figure 1b shows the annual variation in the total number of days with O_3 concentration exceeding the national standard during the period. As shown in Fig. 1a, the monthly mean O_3 concentration in the warm seasons increases over 2014-2018, reaching the maximum of 37.44 ppb in 2017 and maintaining at a high level in 2018. Specifically, O_3 concentration in the YRD shows a large increasing trend of 1.81 ppb (5.21%) per year, which is slightly higher than that in the entire China (5.00% per year, Lu et al. 2020). Meanwhile, the annual average days with O_3 exceeding the standard also show an increasing trend, reaching a peak in 2017 and maintaining at a high level in 2018. In all, both means and extremes of O_3 concentration have increased over the YRD.

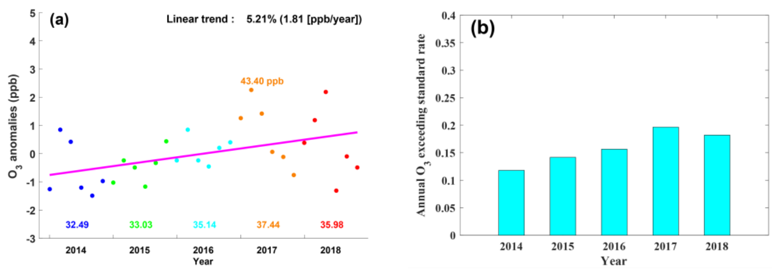

Fig. 1. (a) Anomalies of monthly average O_3 concentration from April to September during 2014–2018. The purple solid line represents the linear fitted curve, and the color number represents the annual (April–September) mean of O_3 concentration. (b) Annual (April–September) variation in the days with O_3 exceeding the national standard.

3.1.2. Characteristics of O_3 variability based on the EOF analysis

https://doi.org/10.5194/acp-2020-902
Preprint. Discussion started: 2 November 2020

In order to further discuss the spatio-temporal distribution characteristics of the observed O_3 concentration, the EOF approach is used to uncover the relationship between the spatial distribution and temporal variation. By removing the missing data for 17 days, O_3 concentrations in 898 days are processed. The percentages of variance contribution for the first three patterns are 65.70 %, 13.80 % and 9.10 %, respectively. The significance tests of the EOF eigenvalue confirm that the first three patterns are significantly separated. Approximately 88.60 % of the variability in the original data is contained in these three patterns. In the first EOF pattern (EOF1), the observed O_3 over the YRD changes similarly and the center of the variation is located in the middle of the YRD (Fig. 2a). As shown in Fig. 2b, the time series of EOF1 presents a decreasing trend and shows a high negative correlation with the time series of O_3 ($R = -0.93$). Therefore, to some extent, the EOF1 time series variation can represent the daily mean O_3 variation during these periods. Considering the negative values in EOF1, the EOF1 time series implies an increasing trend of regional mean O_3 concentration. In addition, the relationships between the time series of EOF1 and different weather systems, as well as the meteorological factors have been investigated. Weather systems include the WPSH and the East Asian summer monsoon, which are dominant weather systems affecting the YRD. Both of them show a poor correlation with the EOF1 time series ($R_{WPSH} = 0.13$ and $R_{EASM} = 0.04$). It indicates that the daily O_3 variation is too complex to be comprehensively explained through the change in a single weather system. Furthermore, the RH presents a good correlation with the EOF1 time series ($R = 0.59$). Han et al. (2020) also found that RH is the most important factor affecting O_3 in the YRD. However, it is still unclear how the change in different weather systems causes the variation in RH, and how the RH variation impacts the other meteorological factors and O_3 accumulation.

In the second EOF pattern (EOF2), there is obvious east-west contrast. In contrast, the third EOF (EOF3) pattern presents a notable south-north contrast. At the same time, the increasing trend of EOF2 time series and the decreasing trend of EOF3 time series indicate that O_3 concentrations in the west and northwest have risen from 2014 to 2018. It implies that a higher rate of O_3 increasing would occur in the northwest. As known, the variance contribution of EOF1 is 65.70 % that is greater than EOF2 (13.80 %) and EOF3 (9.10 %). Therefore, the O_3 increasing in the whole YRD region is the main trend.

https://doi.org/10.5194/acp-2020-902
Preprint. Discussion started: 2 November 2020

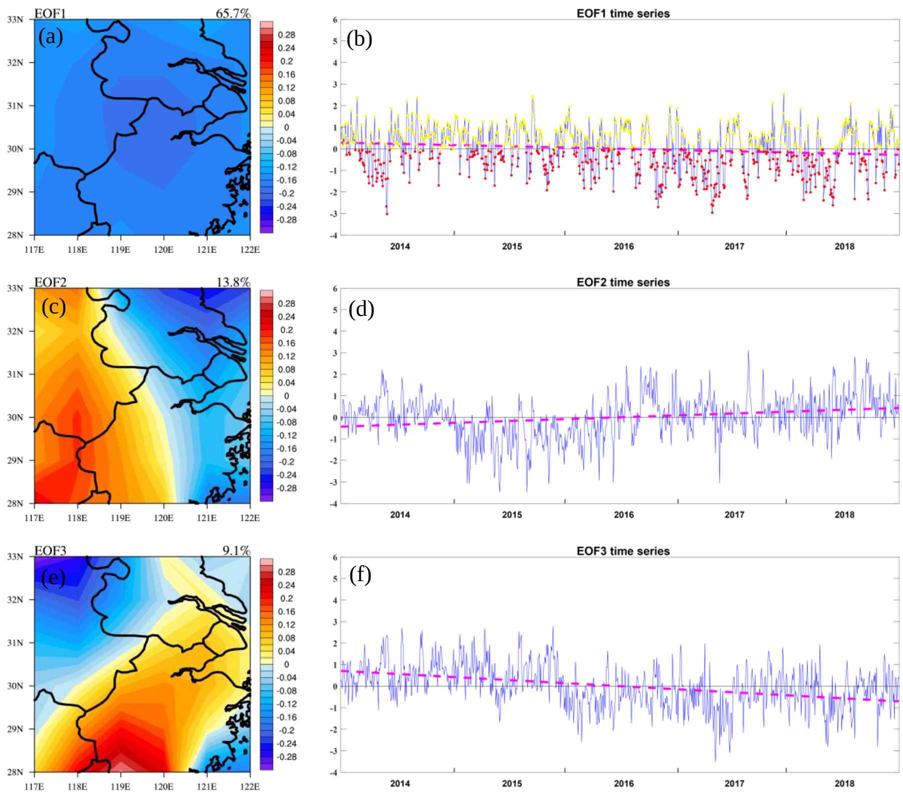

Fig. 2. Three EOF patterns of O_3 concentration in the warm seasons from 2014 to 2018, including the spatial pattern (a, c and e) and time coefficient (b, d and f). The percentage in panels (a, c and e) is the variance contribution of each EOF mode. The orange dash line in panels (b, d and f) represents the linear fitted curve.

3.2. Effects of meteorological conditions on O_3 concentration over the YRD region

3.2.1. Quantifying the effects of meteorological conditions

With the primary pollutant emission being cut down, the O_3 increase might be affected by a variety of factors, one of which was suggested to be the slowing down sink of hydroperoxy radicals, related to the variation in $PM_{2.5}$ (Li et al. 2019). Yet, it is uncertain how meteorological conditions influence this increasing trend. Yang et al. (2019) quantified the meteorological impact on O_3 variation over the Pearl River Delta region using the meteorological adjustment. Similarly

https://doi.org/10.5194/acp-2020-902
Preprint. Discussion started: 2 November 2020

to the methodology in Yang et al. (2019), we investigate the ozone increase over the YRD in the warm seasons during 2014–2018. Fig. 3a shows the ambient O_3 variation from 2014 to 2018: i.e. O_3 concentration increases form 2014, reaches the maximum in 2017, and maintains at a relatively high level in 2018. After the meteorological adjustment, the increasing magnitude is lower than the original one, implying that if the meteorological conditions remained unchanged over the 5 years, the increasing magnitude of ambient O_3 concentration would be lower. The meteorological impact can be examined from the difference between the black solid and dashed lines in Fig. 3a. We focus on periods from the middle of 2014 to the middle of 2018 when the difference is negatively from the middle of 2014 to the middle of 2016 and positively large from middle of 2016 to the meddle of 2018. In 2017, the meteorological conditions increase the O_3 concentration by about 1.20 ppb. However, in 2015, the meteorological conditions become unfavorable to the O_3 accumulation, leading to an O_3 reduction of 1.10 ppb. The meteorological conditions changed the O_3 concentration by 2.81 ppb between the most favorable year (2017) and the most unfavorable year (2015), which roughly corresponds to 9.62% ($\frac{max(MEO\ imapct)-min(MEO\ impact)}{O3(5\ year\ average)}$) of the annual O_3 concentration.

In addition, we select the most influential meteorological factors to discuss their impact on O_3 variation, including T, RH, sunshine duration and wind speed. As shown in Fig. 3b, RH is the most crucial factor and its variation is similar to the variation in the total meteorological impact. Han et al. (2020) also found that RH is the most influential factor in the central and south parts of eastern China. The East Asian summer monsoon plays a key role in affecting the local RH, and meanwhile it might bring a certain amount of O_3 from the south area. However, O_3 concentration is highly negatively related to RH, which implies that the local chemical reaction might contribute more to the O_3 accumulation than the regional transport. The contributions of the other three factors are relatively insignificant.

https://doi.org/10.5194/acp-2020-902
Preprint. Discussion started: 2 November 2020

Atmospheric Chemistry and Physics Discussions

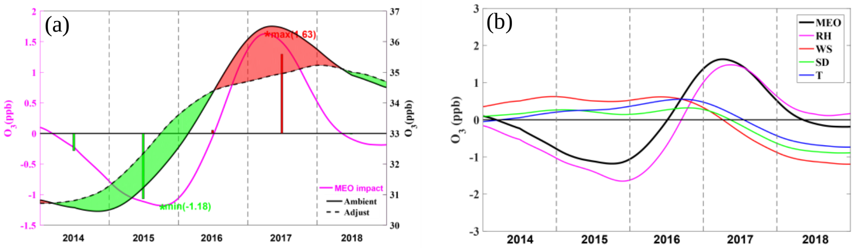

Fig. 3. (a) 5-year trends of ambient O_3 (solid black line), meteorological adjusted O_3 (dashed black line), and the meteorological impact (pink line) over the YRD during 2014–2018. Periods with positive and negative meteorological impacts are shaded with red and green, respectively; red and green bars represent the O_3 increasing and decreasing caused by meteorological conditions in each year. (b) 5-year variations in the meteorological impact of different meteorological factors (MER), including relative humidity (RH), sunshine duration (SR), air temperature (T2) and wind speed (WP).

3.3. Dynamic processes of O_3 variation driven by synoptic circulations

As discussed in section 3.2, the local meteorological factors have a great impact on the O_3 variation. However, to some extent, the variation in local meteorological factors is largely affected by the synoptic-scale weather circulations (Leibensperger et al. 2008; Fiore et al. 2003; Wang et al. 2016). For example, in summer the YRD is under a hot-wet environment controlled by the WPSH. While in winter it is under a cold-dry environment affected by the northwesterly flow caused by the Siberian High. The different weather systems under their corresponding SWPs have their unique meteorological characteristics. Moreover, even under one SWP, the location and intensity changes in a specific weather system can cause the changes in meteorological factors correspondingly (Gao et al. 2020).

3.3.1. The main synoptic weather patterns in the warm season over the YRD

Applying the PTT classification method, nine SWPs are identified for the warm seasons in the YRD. Due to the relatively large variance, the first dominant five types are selected, and the other four types are grouped as ‘other types’. As shown in Table 1, SWP1, SWP2 and SWP4 are

https://doi.org/10.5194/acp-2020-902
Preprint. Discussion started: 2 November 2020

Atmospheric Chemistry and Physics Discussions

dominant, accounting for 40.66%, 22.84% and 13.99% occurances, respectively. In contrast, SWP3, SWP5 and other types are relatively lower, and their occurrence frequencies are 7.65%, 6.99% and 6.01%, respectively. Specifically, SWP1 is affected by the southeasterly flow introduced by the WPSH. SWP2 is influenced by the northwesterly flow introduced by a persistent high pressure. SWP4 is influenced by the southeasterly flow introduced by the WPSH and a cyclone. SWP3 and SWP5 are affected by a cyclone and an anticyclone. For SWP1 and SWP4, it is with high temperature and humidity affected by the southerly flow. But for SWP5, because of the weak northerly flow which brings insufficient water vapor, the YRD is with high temperature and low RH. SWP2 is with relatively lower temperature. SWP3 is under the control of a cyclone and the strong upward motion, it is with weak SR and lower T.

TABLE 1. The occurrence days and frequency, typical characteristics, regional mean ± the standard error for temperature (T), relative humidity (RH), wind speed (WS) and solar radiation (SR) and positive and negative days under each SWP. The > 0 and > 0.5 represent the value of EOF1 time series more than 0 and 0.5, respectively. The < 0 and < 0.5 is on the contrary.

Type and number of days (frequency)	Typical characteristic of SWPs	Meteorological factors	Pos (>0 and >0.5) Neg (<0 and <0.5) (number of days)
SWP1 372 (41.43%)	Southwesterly flow introduced by WPSH	T (℃): 28.38 ± 4.94 RH (%): 77.98 ± 10.44 WS (m/s): 7.30 ± 0.54 SR (W/m^2): 1606.20 ± 537.77	194, 125 175, 112
SWP2 209 (23.27%)	Northwesterly flow introduced by a continuant high pressure	T (℃): 26.40 ± 5.37 RH (%): 73.97 ± 12.85 WS (m/s): 7.28 ± 0.51 SR (W/m^2): 1615.00 ± 563.20	97, 57 110, 73
SWP3 70 (7.80%)	an extratropical cyclone	T (℃): 25.41 ± 4.37 RH (%): 86.80 ± 6.25	58, 45 12, 6

https://doi.org/10.5194/acp-2020-902
Preprint. Discussion started: 2 November 2020

		WS (m/s): 7.33 ± 0.58 SR (W/m^2): 959.73 ± 478.14	
SWP4 128 (14.25%)	Southeasterly flow brought by WPSH and a southern cyclone system	T (℃): 29.29 ± 4.24 RH (%): 78.67 ± 8.51 WS (m/s): 7.11 ± 0.56 SR (W/m^2): 1505.97 ± 538.96	82, 58 46, 30
SWP5 64 (7.13%)	The north China anticyclone system	T (℃): 28.08 ± 4.99 RH (%): 73.97 ± 12.03 WS (m/s): 7.22 ± 0.45 SR (W/m^2): 1586.78 ± 479.65	23, 14 40, 24
others 55 (6.12%)	/	/	/

3.3.2. Impacts of SWP change on O_3 concentration variation

We explore the impacts of SWP change on O_3 variation through combining the EOF1 mode. As illustrated in section 3.1.2, the EOF1 mode is the dominant mode, and it implies the increase of O_3 in the whole area is the main trend. Regarding EOF1 time series, it has a high correlation coefficient with regional O_3 concentration ($R = -0.93$). In this study, we mainly focus on why O_3 concentration increases in the entire YRD region, rather than why the increases in O_3 differ spatially inside the YRD. Therefore, we use the EOF1 time series as a proxy to present the regional O_3 concentration. In Table 1, the positive phase (Pos) represents that the EOF1 time series is more than 0 and it is not beneficial to the production and accumulation of O_3. On the contrary, the negative phase (Neg) means the higher O_3 concentration. We extract the information by comparing Neg with Pos to find the changes of each pattern. Yin et al. (2019) explored dominant patterns of summer O_3 pollution and associated atmospheric circulation changes in eastern China. Different from their study, we have analyzed the daily variation in SWPs, and can obtain the change in atmospheric circulations more precisely.

In the five main SWPs, the EOF1 time series show a decrease trend during their occurrence days in the warm seasons. It means the five main patterns tend to cause high ambient O_3

https://doi.org/10.5194/acp-2020-902
Preprint. Discussion started: 2 November 2020

concentration through the change in SWPs. In addition, the SWP change includes both frequency and intensity changes. We find that the frequency change in SWPs has less impact on the inter-annual variation in O_3 levels than the intensity change in SWPs, which is consistent with the results of Hegarty et al. (2007) and Liu et al. (2019). The contribution of intensity change and frequency change will be further discussed in section 3.4. In the following, we will concretely discuss the variation characteristics of SWPs and their impacts to the increase of O_3 in the YRD.

Fig. 4 shows the atmospheric circulations at 850 hPa and 500 hPa, and the box plot of normalizing factors includes SR, T, TCC, RH, meridional wind at 850hPa (V850) and W (vertical velocity) for SWP1_Pos and SWP1_Neg. As shown in Figs. 4a and 4b, the YRD is located at the northwest of the WPSH, mainly affected by the southwesterly winds. Compared with the SWP1_Pos, the range of WPSH is wider in the northwest area under SWP1_Neg, leading to the strengthened southerly wind in the northwest, which results in higher temperature in this area. Due to the weakening of V850, the water vapor transport acts in response from the south. RH shows a decrease trend. At 500 hPa, a shallow trough is replaced by a slowly moving weak ridge, and the downward motion would strengthen and last longer. The sink motion is favorable for the O_3 accumulation and O_3 photochemical reaction at the near surface. Besides, the decreasing water vapor under the downward motion condition make the cloud cover hard to form. So, stronger solar radiation hits the ground due to the less shelter from the cloud, further leading to higher air temperature and stronger O_3 photochemical reaction.

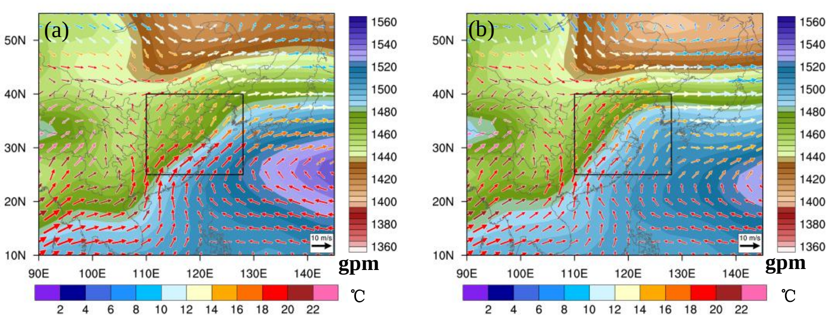

https://doi.org/10.5194/acp-2020-902
Preprint. Discussion started: 2 November 2020

Atmospheric Chemistry and Physics Discussions

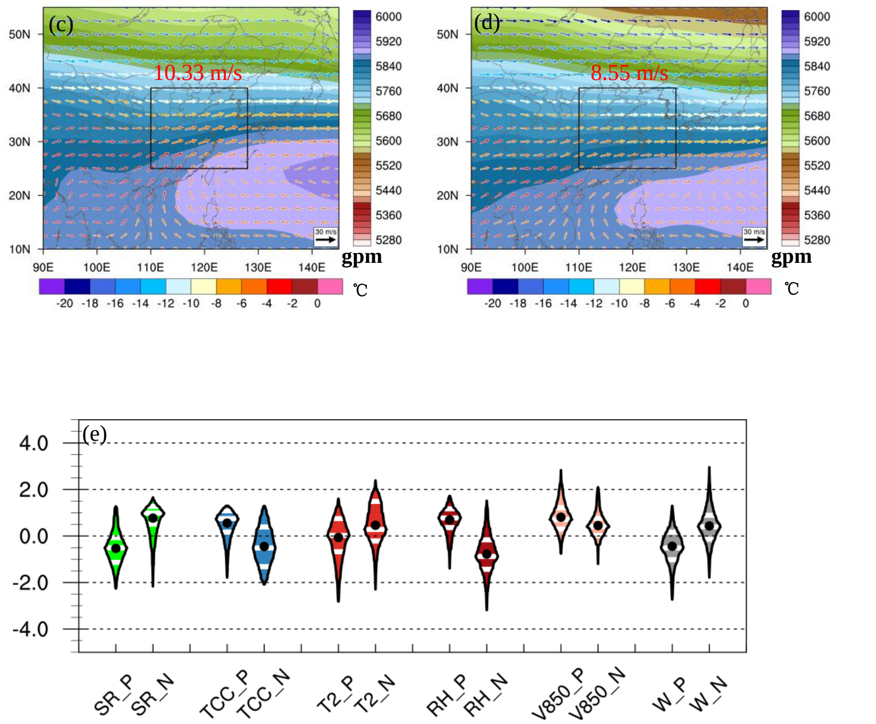

Fig. 4. The geopotential height (shaded) and 850-hPa wind with temperature (color vector) under (a) SWP1_Pos and (b) SWP1_Neg. The geopotential height (shaded) and 500-hPa wind with temperature (color vector) under (c) SWP1_Pos and (d) SWP1_Neg. The red values represent regional average wind speed at 500 hPa in the zone around black lines. (e) The regional average meteorological factors under SWP1_Pos and SWP1_Neg, including SR, TCC, 2-m air temperature, RH, meridional wind at 850 hPa (V850) and W (vertical velocity). The boxed area in Figs.4a-4d encloses the YRD.

Fig. 5 shows the atmospheric circulation structures at 850 hPa and 500 hPa, and the box plot of normalizing factors includes SR, T, TCC, RH, V850 and W for SWP2_Pos and SWP2_Neg. As shown in Figs. 5a and 5b, the YRD is affected by a continental high and the Aleutian low, characterized by northwesterly flow and a bit southwesterly flow. Compared with the SWP2_Pos, the northwesterly flow introduced by the continental high in SWP2_Neg is weaker. At the same time, as the Aleutian low moves southward slightly, the southwesterly flow can hardly bring water

https://doi.org/10.5194/acp-2020-902
Preprint. Discussion started: 2 November 2020

vapor to the YRD, which leads to RH decreases in this area. The correlation between the EOF1 time series and 2-m air temperature under SWP2 (R_{P2} = −0.41) is closer than the correlation in the whole period (R_{all} = −0.24). This implies that the weakening of the continent high plays an important role in enhancing O_3 there. At 500 hPa, a trough is strengthened, leading to the stronger downward motion. Just like SWP1, stronger downward motion and lower RH cause strong SR and high air temperature. All these changes are beneficial to the O_3 formation and accumulation.

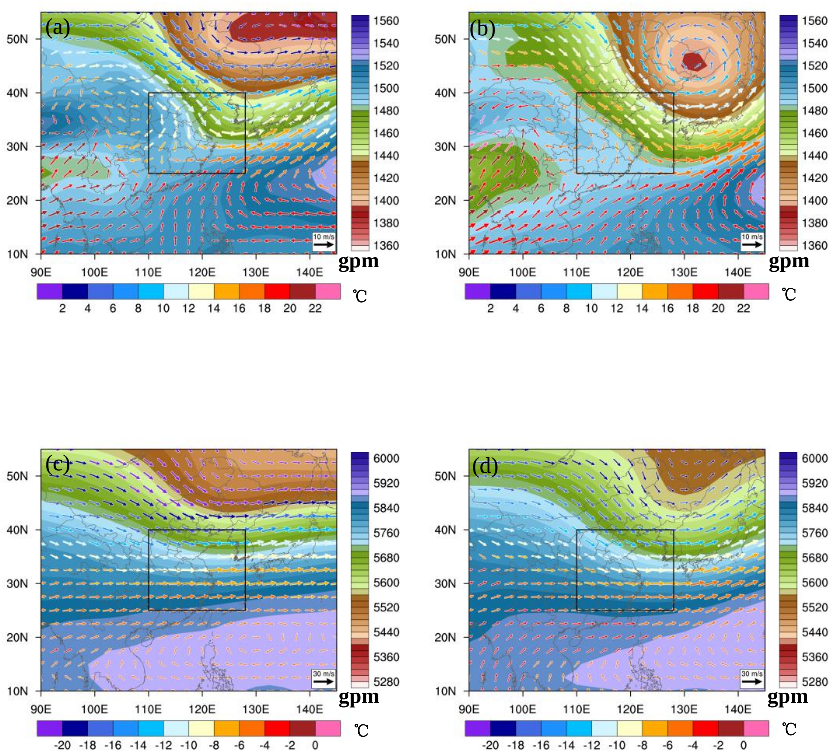

https://doi.org/10.5194/acp-2020-902
Preprint. Discussion started: 2 November 2020

Atmospheric Chemistry and Physics
Discussions

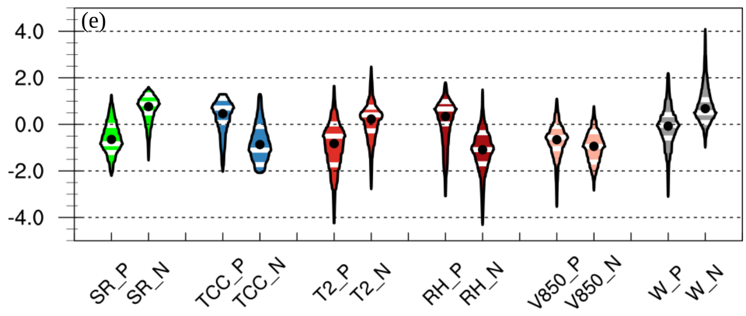

Fig. 5. The geopotential height (shaded) and 850-hPa wind with temperature (color vector) under (a) SWP2_Pos and (b) SWP2_Neg. The geopotential height (shaded) and 500-hPa wind with temperature (color vector) under (c) SWP2_Pos and (d) SWP2_Neg. The red values represent regional average wind speed at 500 hPa in the zone around black lines. (e) The regional average meteorological factors under SWP2_Pos and SWP2_Neg, including SR, TCC, 2-m air temperature, RH, meridional wind at 850 hPa (V850) and W. The boxed area in Figs.5a-5d encloses the YRD.

.

Fig. 6 shows the atmospheric circulations at 850 hPa and 500 hPa, and the box plot of normalizing factors includes SR, T, CC, RH, V850 and W for SWP3_Pos and SWP3_Neg. As shown in Figs. 6a and 6b, the YRD is controlled by an extratropical cyclone. Compared with the SWP3_Pos, the low pressure is lower and its location is slightly further eastward SWP3_Neg. Under this circumstance, the southerly flow at the bottom of the low pressure could hardly bring the water vapor to the YRD. At 500 hPa, the downward motion would be strengthened due to the strengthened trough. The intense downward motion and low RH result in less CC and strong SR, as well as high T, which are instrumental in high O_3 concentration.

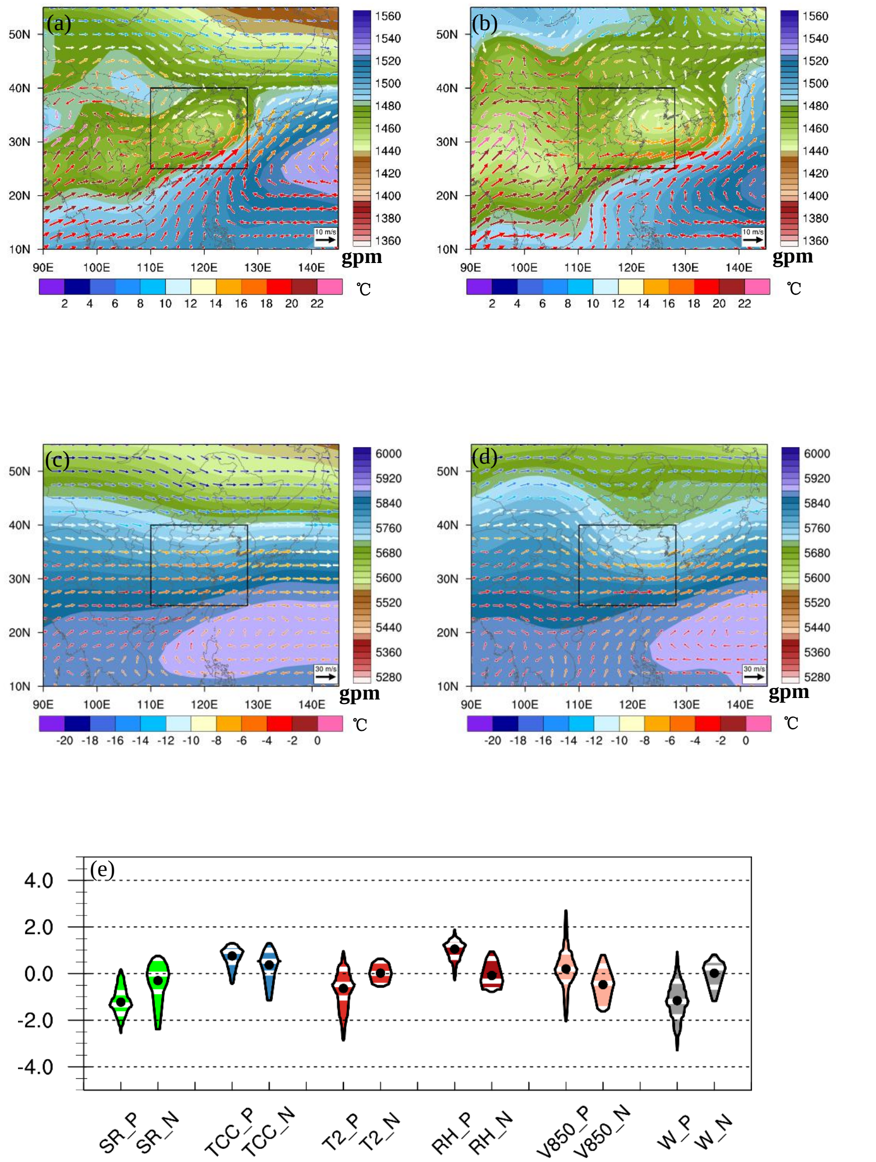

Fig. 6. The geopotential height (shaded) and 850-hPa wind with temperature (color vector) under (a) SWP3_Pos and (b) SWP3_Neg. The geopotential height (shaded) and 500-hPa wind with temperature (color vector) under (c) SWP3_Pos and (d) SWP3_Neg. The red values represent regional average wind speed at 500 hPa in the zone around black lines. (e) The regional average meteorological factors under SWP3_Pos and SWP3_Neg, including SR,

https://doi.org/10.5194/acp-2020-902
Preprint. Discussion started: 2 November 2020

TCC, 2-m air temperature, RH, meridional wind at 850 hPa (V850) and W. The boxed area in Figs6a-6d encloses the YRD.

Fig. 7 shows the atmospheric circulations at 850 hPa and 500 hPa, and the box plot of normalizing factors includes SR, T, TCC, RH, V850 and W for SWP4_Pos and SWP4_Neg. As shown in Figs. 7a and 7b, the southeasterly wins prevails in the YRD, which is caused by a southern low pressure and the WPSH. Compared with the SWP4_Pos, the southern low pressure and southeasterly flow is weaker in SWP4_Neg, and thus it brings less water vapor to the YRD. At 500hPa, a shallow trough strengthens, causing the strong sink motion. High temperature, strong SR and low RH caused by the low V850 and downward motion are favorable for the O_3 accumulation.

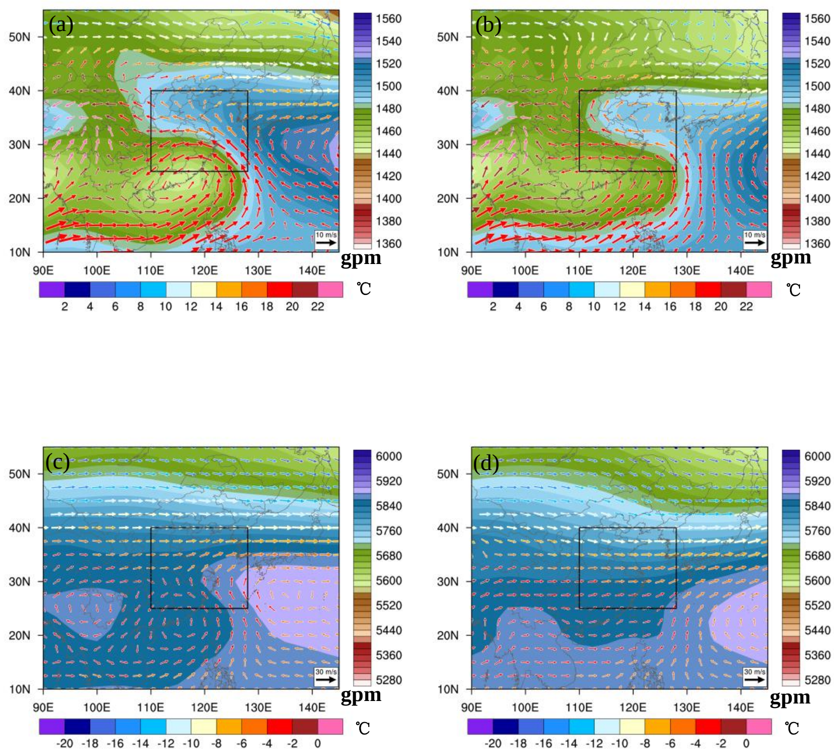

https://doi.org/10.5194/acp-2020-902
Preprint. Discussion started: 2 November 2020

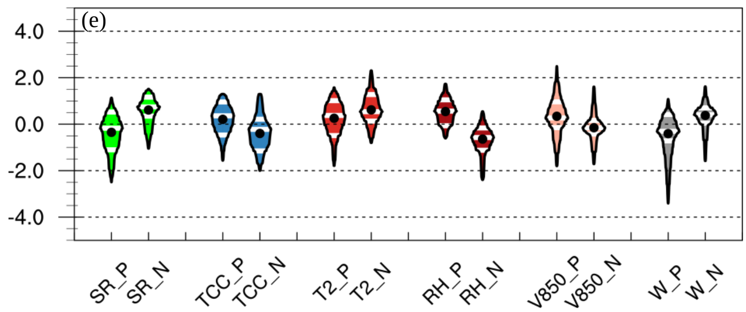

Fig. 7. The geopotential height (shaded) and 850-hPa wind with temperature (color vector) under (a) SWP4_Pos and (b) SWP4_Neg. The geopotential height (shaded) and 500-hPa wind with temperature (color vector) under (c) SWP4_Pos and (d) SWP4_Neg. The red values represent regional average wind speed at 500 hPa in the zone around black lines. (e) The regional average meteorological factors under SWP4_Pos and SWP4_Neg, including SR, TCC, 2-m air temperature, RH, meridional wind at 850 hPa (V850) and W. The boxed area in Figs.7a-7d encloses the YRD.

Fig. 8 shows the atmospheric circulations at 850 hPa and 500 hPa, and the box plot of normalizing factors includes SR, T, TCC, RH, V850 and W for SWP5_Pos and SWP5_Neg. As shown in Figs. 8a and 8b, the YRD is controlled by the north China anticyclone, characterized by the northeasterly and the southwesterly winds. Compared with the SWP5_Pos, the high pressure in the SWP5_Neg is weaker and the northeasterly flow would act in response. The weakened cold sea flow makes the air warmer and dryer. At 500hPa, a trough controlling the YRD would be strengthened. The downward motion would become strong correspondingly. The favorable for the O_3 accumulation.

https://doi.org/10.5194/acp-2020-902
Preprint. Discussion started: 2 November 2020

Atmospheric Chemistry and Physics
Discussions

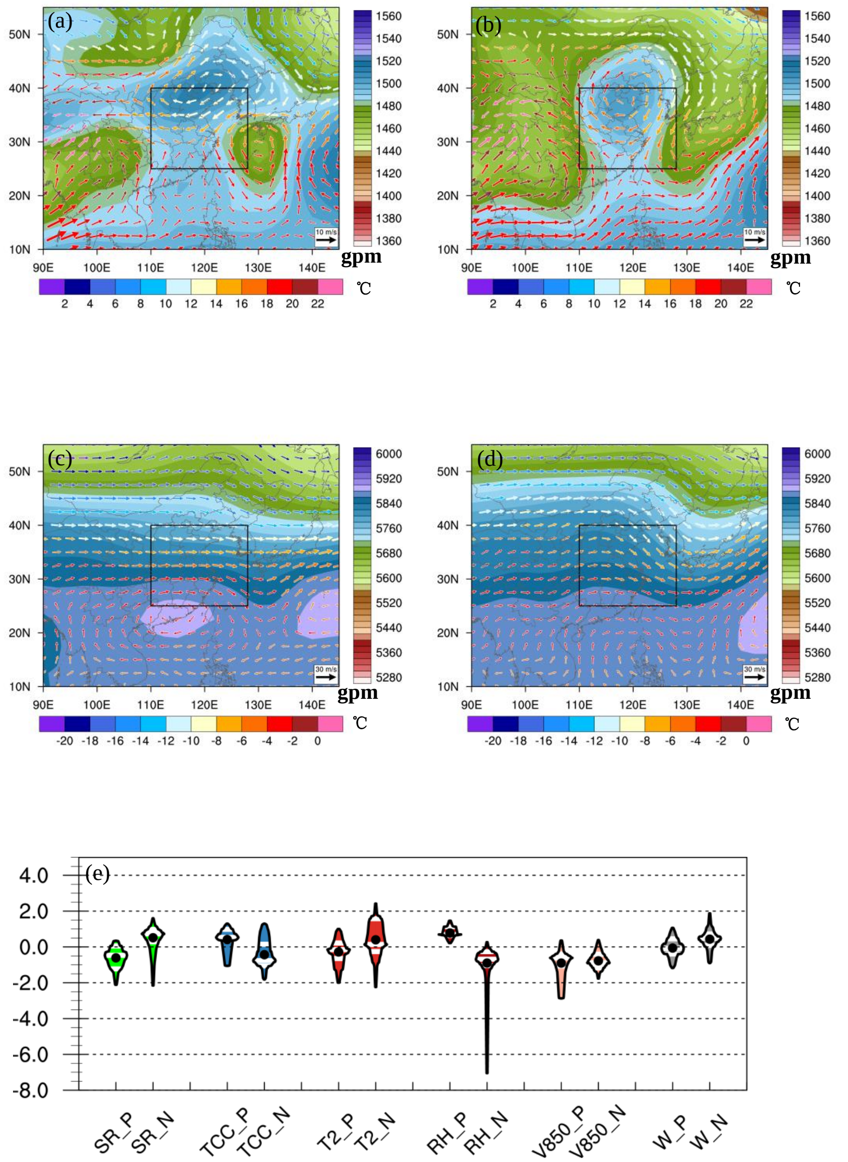

Fig. 8. The geopotential height (shaded) and 850-hPa wind with temperature (color vector) under (a) SWP5_Pos and (b) SWP5_Neg. The geopotential height (shaded) and 500 hPa wind with temperature (color vector) under (c) SWP5_Pos and (d) SWP5_Neg. The red values represent regional average wind speed at 500 hPa in the zone around black lines. (e) The regional average meteorological factors under SWP5_Pos and SWP5_Neg, including SR,

TCC, 2-m air temperature, RH, meridional wind at 850 hPa (V850) and W. The boxed area in Figs.8a-8d encloses the YRD.

3.4. Indicators for reconstructing inter-annual O_3 variation affected by synoptic-scale atmospheric circulation

Due to the similar variations in regional mean O_3 concentration and EOF1 time series, we have reconstructed the inter-annual EOF1 time series to replace the regional mean O_3 concentration by taking into account either frequency-variation-only or both frequency and intensity variations in SWPs, which are EOF1 time series (Fre) and EOF1 time series (Fre + Int), respectively. The observed and reconstructed inter-annual EOF1 time series in 2014–2018 in the whole region are shown in Fig. 9. Obviously, the frequency changes in SWPs almost have no impact on the O_3 variability in the entire YRD. Regarding the intensity change, the fitting curve would be closer to the EOF1 time series. Hegarty et al. (2007) and Liu et al. (2019) reconstructed the inter-annual O_3 level in the northeastern United States and the northern China using the same method as ours. Moreover, they defined the intensity change in SWPs using the domain-averaged sea level pressure and the pressure of the lowest-pressure system. As illustrated by Hegarty et al. (2007), the correlation under Pattern V is poor. It indicates we should select the SWPIIs under each pattern according to their unique characteristics on high O_3 concentration. We select six SWPIIs: the maximum pressure in zone 1 (25°N–40°N, 110°E–130°E) and zone 2 (20°N–50°N, 90°E–140°E), the minimum pressure in zone 1 (25°N–40°N, 110°E–130°E) and zone 2 (20°N–50°N, 90°E–140°E), and the average pressure in zone 1 (25°N–40°N, 110°E–130°E) and zone 3 (10°N –40°N, 110°E–130°E). As shown in Table 2, the SWPII for the maximum pressure in zone 1 has a relative high correlation between SWP3 and SWP5, and the SWPII for the maximum pressure in zone 2 has a relative high correlation between SWP1 and SWP4. The annual EOF1 time series anomalies show a relative good correlation with the maximum pressure. It is because the maximum pressure reflects the wind speed affecting the water vapor transport under this pattern. Compared with SWP3 and SWP5, the synoptic system is larger than the classification region for SWP1 and SWP4. So it can represent the SWPII more precisely in a large region. Under SWP2, when O_3 concentration tends to be at a high level, a cold continent high behind the

https://doi.org/10.5194/acp-2020-902
Preprint. Discussion started: 2 November 2020

YRD would tend to weaken. Therefore, we select the average height in zone 3 to represent the SWPII under SWP2. From Table 2, we can know it has better reconstructed curve when we selected different SWPIIs according to the characteristics of high O_3 level under each pattern. Above all, the intensity change in SWP is more important to the inter-annual O_3 variation than the frequency change.

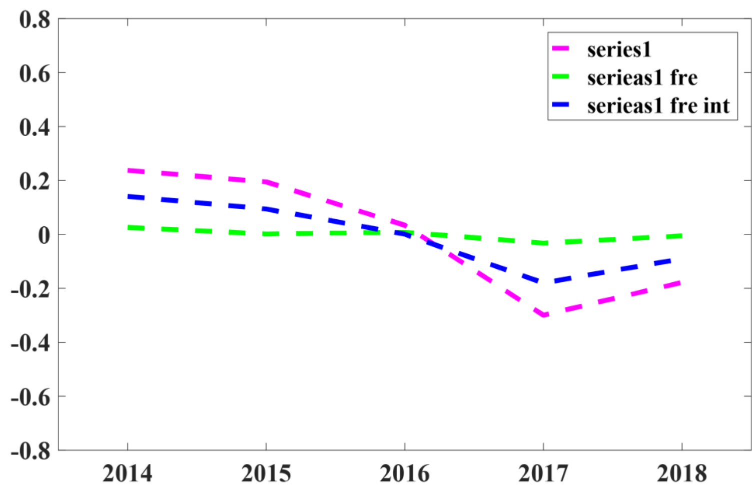

Fig. 9. The original and reconstructed inter-annual EOF1 time series trend based on SWP frequency and intensity variations. The pink curve represents the original inter-annual EOF1 time series, whereas the green and blue lines are the trends of reconstructed inter-annual EOF1 time series according to the frequency-variation-only and both frequency and intensity variations in SWPs, respectively.

TABLE 2. Correlation coefficients between EOF1 time series and different SWPIIs under each SWP.

Type	$Z_{1\text{-ave}}$	$Z_{1\text{-max}}$	$Z_{1\text{-min}}$	$Z_{2\text{-min}}$	$Z_{2\text{-max}}$	$Z_{3\text{-ave}}$
SWP1	-0.47	-0.29	-0.35	-0.33	-0.60	-0.32
SWP2	-0.14	-0.08	0.02	-0.07	-0.09	-0.40
SWP3	0.28	0.61	0.03	0.005	0.43	-0.60
SWP4	-0.14	-0.03	-0.17	-0.22	0.78	-0.38

https://doi.org/10.5194/acp-2020-902
Preprint. Discussion started: 2 November 2020

SWP5	0.52	0.76	0.39	0.56	0.72	0.58

4. Conclusions and discussions

In this study, we discussed the meteorological influences on the O_3 variation in the warm seasons during 2014–2018 in the YRD, China. Specifically, we analyzed the O_3 spatio-temporal distribution characteristics, quantified the contribution of meteorological conditions to O_3 variations, explored how the change in SWPs and corresponding meteorological factors lead to O_3 increase over 2014-2018, and quantitatively analyzed the impact of SWP frequency and intensity on the inter-annual O_3 variation. The main conclusions are as follows.

The annual regional averaged O_3 concentrations from 2014 to 2018 in the YRD are 32.49, 33.03, 35.14, 37.44 and 35.98 ppb, respectively, with a significantly increasing rate of 1.81 ppb year^{-1} (5.21% year^{-1}). At the same time, the total number of days on which O_3 concentration exceeds the national standard also increases with year in a similar pattern. Through the EOF analysis of O_3 in space and time, three dominant modes were identified. The first mode is the most dominant mode, accounting for 65.7% of O_3 variation, implying that the O_3 increasing in the entire YRD is the main tendency. A high correlation coefficient between the EOF1 time series and RH (R_{rh} = 0.59) indicates that RH is the most influential factor leading to the O_3 increase.

We quantified the influence of meteorology on inter-annual variation and trend of O_3 over the YRD from 2014-2018, and found that the influence could lead to a regional O_3 increase by 2.81 ppb at most. Especially, RH plays the most important role in modulating the inter-annual O_3 variation. Moreover, in order to explore connections between the O_3 variation and synoptic circulations, nine types of SWPs were objectively identified based on the PTT method, and five main types were selected to correlate with the EOF1 time series. We found that the variation in all SWPs over 2014-2018 are favorable to O_3 increase in that period. The variation in SWP intensity include the WPSH weakening and northward extending under SWP1, a continent high weakening under SWP2, an extratropical cyclone strengthening under SWP3, the southern low pressure weakening and the WPSH weakening under SWP4, and the north China anticyclone weakening under SWP5. All these changes prevent the water vapor from being transported to the YRD and increase air temperature in YRD. In addition, the downward motions strengthen in the YRD,

https://doi.org/10.5194/acp-2020-902
Preprint. Discussion started: 2 November 2020

which is behind the trough and in front of the ridge due to the strengthening of the ridge and trough, leading to less cloud cover and stronger SR. All of these are favorable to O_3 formation and accumulation.

We found that the change in SWPs intensity is more important to the O_3 increase over 2014-2018 than that in SWPs frequency. We further reconstructed the EOF1 time series by considering different SWPIIs due to the unique characteristics of each SWP. The results are better than those in Hegarty et al. (2007) and Liu et al. (2019) who used the same SWPIIs in all SWPs.

In summary, this study quantified the inter-annual variation and increasing rate of O_3 in the YRD, China, and explored the connection between SWP variations and the O_3 increase. It provides an enhanced understanding of response of O_3 variation to changes in SWPs from year to year and thus this understanding may be insightful to planning strategies for O_3 pollution control.

Authorship contribution statement

Da Gao: Conceptualization, Data curation, Formal analysis, Meteorology, Investigation, software, Writing – original draft, Writing – revision. **Min Xie**: Conceptualization, Methodology, Writing – revision, Project administration, Funding acquisition. **Jane Liu:** Formal analysis, Meteorology, Writing – revision. **Tijian Wang**: Formal analysis, Funding acquisition. **Chaoqun Ma**: Formal analysis, Meteorology. **Haokun Bai**: Formal analysis, Meteorology. **Xing Chen**: Formal analysis.

Declaration of competing interest

The authors declare that they have no known competing financial interests or personal relationships that could have appeared to influence the work reported in this paper.

Acknowledgements

This work was supported by the National Key Research and Development Program of China (2018YFC0213502, 2018YFC1506404).

References

Barnes, E. A., and Fiore, A. M.: Surface ozone variability and the jet position: Implications for projecting

https://doi.org/10.5194/acp-2020-902
Preprint. Discussion started: 2 November 2020

future air quality, Geophys Res Lett, 40, 2839-2844, 10.1002/grl.50411, 2013.

Cooper, O. R., Schultz, M. G., Schroder, S., Chang, K. L., Gaudel, A., Benitez, G. C., Cuevas, E., Frohlich, M., Galbally, I. E., Molloy, S., Kubistin, D., Lu, X., McClure-Begley, A., Nedelec, P., O'Brien, J., Oltmans, S. J., Petropavlovskikh, I., Ries, L., Senik, I., Sjoberg, K., Solberg, S., Spain, G. T., Spangl, W., Steinbacher, M., Tarasick, D., Thouret, V., and Xu, X. B.: Multi-decadal surface ozone trends at globally distributed remote locations, Elementa-Sci Anthrop, 8, Artn 23 10.1525/Elementa.420, 2020.

Day, D. B., Xiang, J., and Mo, J.: Association of ozone exposure with cardiorespiratory pathophysiologic mechanisms in healthy adults (vol 177, pg 1344, 2017), Jama Intern Med, 177, 1400-1400, 10.1001/jamainternmed.2017.4605, 2017.

Doherty, R. M., Wild, O., Shindell, D. T., Zeng, G., MacKenzie, I. A., Collins, W. J., Fiore, A. M., Stevenson, D. S., Dentener, F. J., Schultz, M. G., Hess, P., Derwent, R. G., and Keating, T. J.: Impacts of climate change on surface ozone and intercontinental ozone pollution: A multi-model study, J Geophys Res-Atmos, 118, 3744-3763, 10.1002/jgrd.50266, 2013.

Eskridge, R. E., Ku, J. Y., Rao, S. T., Porter, P. S., and Zurbenko, I. G.: Separating different scales of motion in time series of meteorological variables, B Am Meteorol Soc, 78, 1473-1483, Doi 10.1175/1520-0477(1997)078<1473:Sdsomi>2.0.Co;2, 1997.

Fiore, A. M., Jacob, D. J., Mathur, R., and Martin, R. V.: Application of empirical orthogonal functions to evaluate ozone simulations with regional and global models, J Geophys Res-Atmos, 108, Artn 4431 10.1029/2002jd003151, 2003.

Gao, D., Xie, M., Chen, X., Wang, T. J., Liu, J., Xu, Q., Mu, X. Y., Chen, F., Li, S., Zhuang, B. L., Li, M. M., Zhao, M., and Ren, J. Y.: Systematic classification of circulation patterns and integrated analysis of their effects on different ozone pollution levels in the Yangtze River Delta Region, China, Atmos Environ, https://doi.org/10.1016/j.atmosenv.2020.117760 2020.

Gao, W., Tie, X. X., Xu, J. M., Huang, R. J., Mao, X. Q., Zhou, G. Q., and Chang, L. Y.: Long-term trend of O_3 in a mega City (Shanghai), China: Characteristics, causes, and interactions with precursors, Sci Total Environ, 603, 425-433, 10.1016/j.scitotenv.2017.06.099, 2017.

Han, H., Liu, J. E., Shu, L., Wang, T. J., and Yuan, H. L.: Local and synoptic meteorological influences on daily variability in summertime surface ozone in eastern China, Atmos Chem Phys, 20, 203-222, 10.5194/acp-20-203-2020, 2020.

He, J. J., Gong, S. L., Yu, Y., Yu, L. J., Wu, L., Mao, H. J., Song, C. B., Zhao, S. P., Liu, H. L., Li, X. Y., and Li, R. P.: Air pollution characteristics and their relation to meteorological conditions during 2014-2015 in major Chinese cities, Environ Pollut, 223, 484-496, 10.1016/j.envpol.2017.01.050, 2017.

Hegarty, J., Mao, H., and Talbot, R.: Synoptic controls on summertime surface ozone in the northeastern United States, J Geophys Res-Atmos, 112, Artn D14306 10.1029/2006jd008170, 2007.

Hou, X. W., Zhu, B., Kumar, K. R., and Lu, W.: Inter-annual variability in fine particulate matter pollution over China during 2013-2018: Role of meteorology, Atmos Environ, 214, ARTN 116842 10.1016/j.atmosenv.2019.116842, 2019.

Jacob, D. J., and Winner, D. A.: Effect of climate change on air quality, Atmos Environ, 43, 51-63, 10.1016/j.atmosenv.2008.09.051, 2009.

Jacob, D. J., and Winner, D. A.: Effect of climate change on air quality, Atmos Environ, 43, 51-63, 2009.

Jerrett, M., Burnett, R. T., Pope, C. A., Ito, K., Thurston, G., Krewski, D., Shi, Y. L., Calle, E., and Thun, M.: Long-Term Ozone Exposure and Mortality., New Engl J Med, 360, 1085-1095, Doi 10.1056/Nejmoa0803894, 2009.

Jin, X. M., and Holloway, T.: Spatial and temporal variability of ozone sensitivity over China observed from the Ozone Monitoring Instrument, J Geophys Res-Atmos, 120, 7229-7246, 10.1002/2015JD023250, 2015.

Leibensperger, E. M., Mickley, L. J., and Jacob, D. J.: Sensitivity of US air quality to mid-latitude cyclone frequency and implications of 1980-2006 climate change, Atmos Chem Phys, 8, 7075-7086, DOI 10.5194/acp-8-7075-2008, 2008.

Li, K., Jacob, D. J., Liao, H., Shen, L., Zhang, Q., and Bates, K. H.: Anthropogenic drivers of 2013-2017 trends in summer surface ozone in China, P Natl Acad Sci USA, 116, 422-427, 2019.

Liu, J. D., Wang, L. L., Li, M. G., Liao, Z. H., Sun, Y., Song, T., Gao, W. K., Wang, Y. H., Li, Y., Ji, D. S., Hu, B., Kerminen, V. M., Wang, Y. S., and Kulmala, M.: Quantifying the impact of synoptic circulation patterns on ozone variability in northern China from April to October 2013-2017, Atmos Chem Phys, 19, 14477-14492, 10.5194/acp-19-14477-2019, 2019.

Lu, X., Hong, J. Y., Zhang, L., Cooper, O. R., Schultz, M. G., Xu, X. B., Wang, T., Gao, M., Zhao, Y. H., and Zhang, Y. H.: Severe Surface Ozone Pollution in China: A Global Perspective, Environ Sci Tech Let, 5, 487-494, 10.1021/acs.estlett.8b00366, 2018.

Lu, X., Zhang, L., Chen, Y. F., Zhou, M., Zheng, B., Li, K., Liu, Y. M., Lin, J. T., Fu, T. M., and Zhang, Q.: Exploring 2016-2017 surface ozone pollution over China: source contributions and meteorological influences, Atmos Chem Phys, 19, 8339-8361, 10.5194/acp-19-8339-2019, 2019.

Lu, X., Zhang, L., Wang, X. L., Gao, M., Li, K., Zhang, Y. Z., Yue, X., and Zhang, Y. H.: Rapid Increases in Warm-Season Surface Ozone and Resulting Health Impact in China Since 2013, Environ Sci Tech Let, 7, 240-247, 10.1021/acs.estlett.0c00171, 2020.

Milanchus, M. L., Rao, S. T., and Zurbenko, I. G.: Evaluating the effectiveness of ozone management efforts in the presence of meteorological variability, J Air Waste Manage, 48, 201-215, Doi 10.1080/10473289.1998.10463673, 1998.

Papanastasiou, D. K., Melas, D., Bartzanas, T., and Kittas, C.: Estimation of Ozone Trend in Central Greece, Based on Meteorologically Adjusted Time Series, Environ Model Assess, 17, 353-361, 10.1007/s10666-011-9299-6, 2012.

Philipp, A., Beck, C., Huth, R., and Jacobeit, J.: Development and comparison of circulation type classifications using the COST 733 dataset and software, Int J Climatol, 36, 2673-2691, 10.1002/joc.3920, 2016.

Pu, X., Wang, T. J., Huang, X., Melas, D., Zanis, P., Papanastasiou, D. K., and Poupkou, A.: Enhanced surface ozone during the heat wave of 2013 in Yangtze River Delta region, China, Sci Total Environ, 603, 807-816, 10.1016/j.scitotenv.2017.03.056, 2017.

Rao, S. T., and Zurbenko, I. G.: Detecting And Tracking Changes In Ozone Air-Quality, J Air Waste Manage, 44, 1089-1092, Doi 10.1080/10473289.1994.10467303, 1994.

Rao, S. T., and Zurbenko, I. G.: Detecting And Tracking Changes In Ozone Air-Quality, J Air Waste Manage, 44, 1089-1092, Doi 10.1080/10473289.1994.10467303, 1994.

Shu, L., Xie, M., Wang, T. J., Gao, D., Chen, P. L., Han, Y., Li, S., Zhuang, B. L., and Li, M. M.: Integrated studies of a regional ozone pollution synthetically affected by subtropical high and typhoon system in the Yangtze River Delta region, China, Atmos Chem Phys, 16, 15801-15819, 10.5194/acp-16-15801-2016, 2016.

Shu, L., Xie, M., Gao, D., Wang, T. J., Fang, D. X., Liu, Q., Huang, A. N., and Peng, L. W.: Regional severe particle pollution and its association with synoptic weather patterns in the Yangtze River Delta region, China, Atmos Chem Phys, 17, 12871-12891, 10.5194/acp-17-12871-2017, 2017.

Tong, L., Zhang, H. L., Yu, J., He, M. M., Xu, N. B., Zhang, J. J., Qian, F. Z., Feng, J. Y., and Xiao, H.:

https://doi.org/10.5194/acp-2020-902
Preprint. Discussion started: 2 November 2020

Characteristics of surface ozone and nitrogen oxides at urban, suburban and rural sites in Ningbo, China, Atmos Res, 187, 57-68, 2017.

Wang, T., Xue, L. K., Brimblecombe, P., Lam, Y. F., Li, L., and Zhang, L.: Ozone pollution in China: A review of concentrations, meteorological influences, chemical precursors, and effects, Sci Total Environ, 575, 1582-1596, 10.1016/j.scitotenv.2016.10.081, 2017.

Wise, E. K., and Comrie, A. C.: Extending the Kolmogorov-Zurbenko filter: Application to ozone, particulate matter, and meteorological trends, J Air Waste Manage, 55, 1208-1216, Doi 10.1080/10473289.2005.10464718, 2005.

Xie, M., Zhu, K. G., Wang, T. J., Yang, H. M., Zhuang, B. L., Li, S., Li, M. G., Zhu, X. S., and Ouyang, Y.: Application of photochemical indicators to evaluate ozone nonlinear chemistry and pollution control countermeasure in China, Atmos Environ, 99, 466-473, 10.1016/j.atmosenv.2014.10.013, 2014.

Yang, Y., Liao, H., and Li, J.: Impacts of the East Asian summer monsoon on interannual variations of summertime surface-layer ozone concentrations over China, Atmos Chem Phys, 14, 6867-6879, 2014.

Yang, L. F., Luo, H. H., Yuan, Z. B., Zheng, J. Y., Huang, Z. J., Li, C., Lin, X. H., Louie, P. K. K., Chen, D. H., and Bian, Y. H.: Quantitative impacts of meteorology and precursor emission changes on the long-term trend of ambient ozone over the Pearl River Delta, China, and implications for ozone control strategy, Atmos Chem Phys, 19, 12901-12916, 10.5194/acp-19-12901-2019, 2019.

Yarnal, B.: Synoptic Climatology in Environmental Analysis A Primer, Journal of Preventive Medicine Information, 347, 170-180, 1993.

Yin, Z. C., Cao, B. F., and Wang, H. J.: Dominant patterns of summer ozone pollution in eastern China and associated atmospheric circulations, Atmos Chem Phys, 19, 13933-13943, 10.5194/acp-19-13933-2019, 2019.

Yue, X., Unger, N., Harper, K., Xia, X. G., Liao, H., Zhu, T., Xiao, J. F., Feng, Z. Z., and Li, J.: Ozone and haze pollution weakens net primary productivity in China, Atmos Chem Phys, 17, 6073-6089, 10.5194/acp-17-6073-2017, 2017.

Zhang, J. X., Gao, Y., Luo, K., Leung, L. R., Zhang, Y., Wang, K., and Fan, J. R.: Impacts of compound extreme weather events on ozone in the present and future, Atmos Chem Phys, 18, 9861-9877, 10.5194/acp-18-9861-2018, 2018.

Zhao, Z. J., and Wang, Y. X.: Influence of the West Pacific subtropical high on surface ozone daily variability in summertime over eastern China, Atmos Environ, 170, 197-204, 2017.